Title
Automatic Segmentation and Quantification of Kinematics in Patients with ACL Injuries

Author
Huang, Samuel

Publication Date
2015

Peer reviewed|Thesis/dissertation

Automatic Segmentation and Kinematic Quantification of ACL Injured Patients Knees

by

Samuel Huang

THESIS

Submitted in partial satisfaction of the requirements for the degree of

MASTER OF SCIENCE

in

Biomedical Imaging

in the

GRADUATE DIVISION

of the

UNIVERSITY OF CALIFORNIA, SAN FRANCISCO

[redacted]

Acknowledgements

I would like to thank Dr. Xiaojuan Li for guidance and for providing the means to take on this thesis project. She helped me to expand my vision in research and to strive for goals I would have otherwise shied away from. Dr. Valentina Pedoia was very gracious to me during this project, spending many hours going over issues both big and small. I'd like to thank advisors Dr. Richard Souza and Dr. Thomas Link for their support and guidance as well.

I'd like to thank my parents, Neng and Helen Huang, and my sister Christina, who have been lifelong examples of love and self-sacrifice. Lastly I'd like to give thanks and glory to the Lord Jesus Christ who in this particular season has taught me the joy of service and the importance of perseverance.

Automatic Segmentation and Quantification of Kinematics in Patients with ACL Injuries

Samuel Huang

Objectives: To develop an automated intra-patient atlas based bone segmentation technique that is reliable for the quantification of in-vivo MRI knee kinematics.

Materials and Methods: 30 patients who had unilateral anterior cruciate ligament (ACL) tear and under went ACL single-bundle reconstruction received loaded-MRI scans. The same procedure was done for 6 healthy control patients for reproducibility. Femur and tibia were segmented automatically, and using in-house MATLAB software, three-dimensional segmentations were used to obtain kinematic data (Internal Tibial Rotation [ITR] and Tibial Position [TP]). Automatic segmentation and kinematic data was compared to results from previously used semi-automatic segmentation methods.

Results: Automatic segmentation was successful in 98.9% of 175 cases tested, with high similarity between masks of automatic and semi-automatic segmentation (85.1%). Automatic segmentation algorithm showed excellent reproducibility results between scan and rescan segmentations with an average absolute difference of: TP: 0.46 +/- 0.41 mm, ITR: 1.60 +/- 1.58 deg. These values were superior to those obtained semi-automatically. Automatic and semi-automatic kinematic results showed high correlation for both TP and ITR, with R=0.935 and R=0.900 respectively. [add summary of longitudinal changes of TP and ITR in patients]

Conclusions: The automatic segmentation technique developed in this paper proves to be very useful in reducing segmentation time and labor as well as in reducing user-generated bias. The proposed technique demonstrates a highly consistent and robust method that is useful for longitudinal knee kinematics quantification for in-vivo MRI.

Table of Contents

List of Figures and Tables

Figures

Tables

1. Introduction

1.1 Clinical Issue: Osteoarthritis among patients with ACL Injuries / The Role of Knee Kinematics

Numerous studies have provided evidence that traumatic anterior-cruciate ligament (ACL) injury is highly correlated with the early onset of osteoarthritis [1-2]. Additionally it has been found that patients with ACL reconstruction are no less likely to develop premature osteoarthritis than those without reconstructive surgery [1]. Researchers have theorized that pre-mature osteoarthritis that is common among those with ACL tear may be caused by altered kinematics of the knee. Interestingly enough, studies have shown that ACL-reconstructed knees frequently exhibit kinematics more similar to an ACL-deficient knees than healthy ones [2]. The ACL plays a vital role in kinematics, as it facilitates both extension-flexion motions and rotation motions about the knee joint. The changes in kinematics after injury can cause abnormal knee cartilage loading patterns leading to rapid degeneration of cartilage [2]. Keeping these things in mind, it is essential that researchers discover more about the relationships between kinematics and knee osteoarthritis development. The restoration of knee kinematics in injured patients may end up being a critical component in preventing osteoarthritis in early stages.

1.2 Clinical Approaches: The Necessity of Kinematic Restoration and Quantitative Techniques

Current ACL reconstruction techniques are primarily focused on returning the patient to previous lifestyle or sport activity. None of these surgical procedures, however, have been known to deter cartilage degeneration [7]. If indeed the change in knee kinematics is a primary factor in knee cartilage degeneration, it is essential to develop meaningful quantitative methods to assess those kinematic changes. These methods will enable researchers to track kinematic changes over time in conjunction with potential early osteoarthritic symptoms. In addition, specific types of kinematic changes may be identified as primary initiators of osteoarthritis. Once those factors are identified, clinicians can begin to develop methods targeted at those specific problems.

1.3 Current Methods: MRI for In-vivo Quantitative Kinematics Measurements

Recently, MRI has emerged as an advantageous imaging modality for the measurement of knee kinematics [3][8]. It is beneficial because of its spatial resolution, absence of harmful radiation, and most importantly its capability of non-invasive in vivo imaging of soft tissue. There are some potential drawbacks however. The acquisition times are relatively long, increasing the chance of motion artifacts, and potentially causing problems with acquiring good images. Nevertheless, MRI has shown great promise in early studies. One such study is done through acquiring a patient MRI while the patient bears an axially load as a percentage of their body weight to the knee joint through the foot [8]. From the MRI acquisition, three-dimensional models can be constructed to measure the kinematics of the tibia relative to the femur. Two particular parameters of interest are 1) tibial position: the position of the tibia relative to the femur, and 2) internal tibial rotation: the internal rotation of the tibia relative to the femur. These variables relate closely to the primary functions of the ACL are among the most discussed in the study of knee kinematics.

1.4 Bone Segmentation: A Critical Step in Quantitative Kinematic MRI Methods

Before quantitative kinematic data from patient MRI can be acquired, the tibia and femur bones must be identified within the 3-D image. This process of identifying the region of interest, called segmentation, is a crucial step in the quantification process. The accuracy of bone segmentation will directly affect the kinematic information obtained. That being said, segmentation is not a trivial task. Oftentimes segmentation requires extensive operator input.

This is undesirable for two major reasons. The first is that the cost in time and labor is very high. An average knee MRI acquisition takes on the order of hours to segment. Such a repetitive and tedious process is sure to wear down even the most enthusiastic researcher. The other problem is that non-automated segmentation is difficult to reproduce, especially between different segmentation operators. Even persons who are trained in the same manner will likely interpret certain boundaries differently. These problems with manual or semi-automatic segmentation can become a choke point in the data analysis process and can dramatically reduce the pace of research development. Improved segmentation methods that require minimal or no user input would lift the burden of labor in the segmentation process, and would be more consistent and reproducible with minimal or no operator related bias.

1.5 Study Motivation and Goals

Because of the challenges of segmentation mentioned previously, the methods discussed in this thesis were devised to produce an automatic segmentation method that is reliable for the quantification of knee kinematics. It is the hope of the author that by using these methods researchers can reach meaningful clinical conclusions sooner and ultimately bring an increased level of care to patients in need.

2. Methods

2.1 Patient recruitment and case selection:

30 subjects with unilateral ACL tear were included in this study. There were 15 males and 15 females with: mean age of 30.3 ± 8.4 years, Height of 1.72 ± .09 meters, Weight of 70.98 ± 13.02 kg, and BMI of 23.77 ± 2.85 kg/m^2. All subjects injured knees were reconstructed by single bundle reconstruction surgery. These subjects were followed for at least two years after surgery.

In addition, 6 healthy subjects (3 male, 3 female) from previous published study [3] were included to compare the reproducibility of automatic segmentation algorithm to semi-automatic segmentation methods previously used. These subjects had a mean age of 26.7 ± 0.82 years.

2.2 Image acquisition and Imaging parameters:

Figure 1. Typical T2-weighted fast spin echo images acquired during loaded-MRI

Subjects with ACL injury underwent MRI scans at 4 different time points (Fig. 2): 1) after ACL injury and before surgery (baseline), 2) 6 months after surgical reconstruction, 3) 1 year after surgical reconstruction, 4) 2 years after surgical reconstruction. Separate MRI scans of bi-lateral knees were taken while patients bore 25% body weight and kept an extended leg position throughout the scan. All scans were acquired in the sagittal plane by a T2 weighted fast spin echo sequence on a 3T wide-bore MR Scanner (GE Healthcare; Waukesha, WI) using an 8-channel knee coil. Imaging parameters were prescribed as follows: Field of view = 20 cm; matrix size = 512 x 512; pixel size = 0.39 mm x 0.39 mm; slice thickness = 1.5 mm, TR = 4000 ms, TE = 48.16 ms.

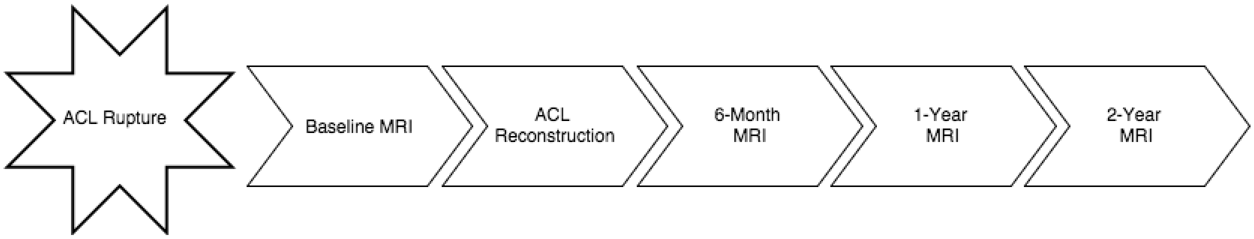

Figure 2. Timeline of subjects throughout the study

The six healthy subjects were scanned twice for reproducibility analysis, with each patient exiting the scan room for a brief period of time before being rescanned in similar fashion. The method of image acquisition was the same as for the group previously described.

2.3 Segmentation of Bone Geometry

Segmentation Overview:

An automatic segmentation algorithm for the tibia and femur was developed in this study based on an intra-patient atlas-based method [5]. Baseline segmentations of femur and tibia performed previously using a semi-automatic method were used as a template for follow-up automatic segmentation. By registering baseline MRI to follow-up MRI using a three-dimensional non-rigid B-spline transformation, transformation coordinates mapping the two images were obtained. This allows for baseline segmentations to be spatially transformed to fit the follow-up MRI. The kinematics of the joint was then quantified using the 3D segmentation of femur and tibia. An outline of segmentation and kinematic quantification process is outlined in Fig. 3. The following sections will explain the finer details of the segmentation process.

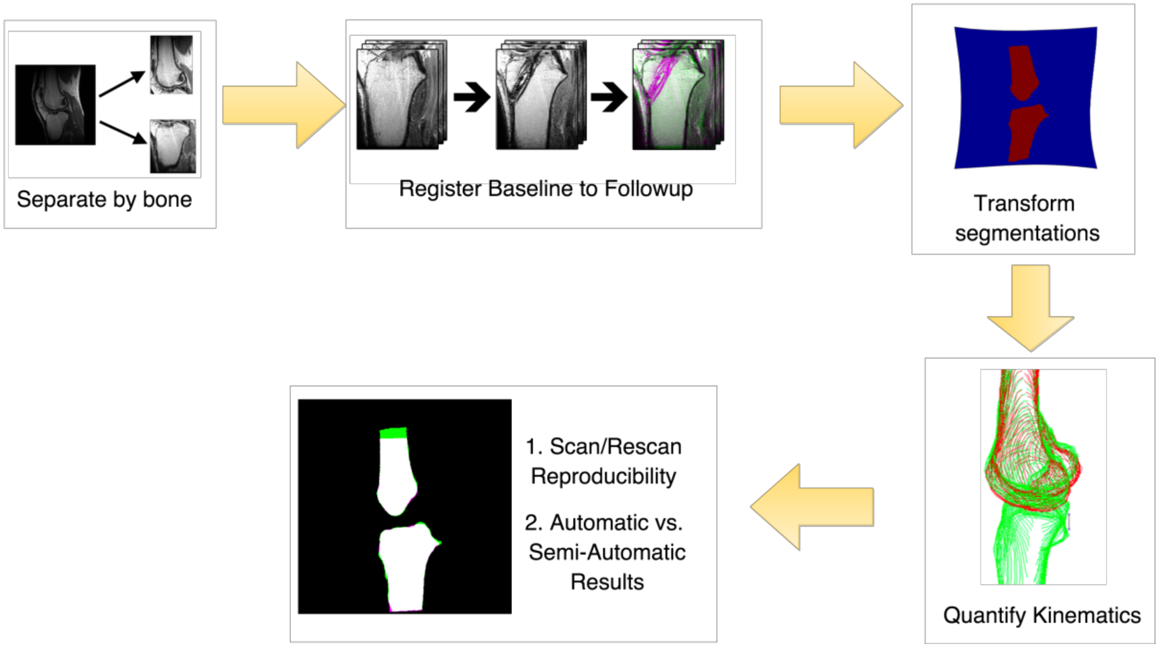

Figure 3. Diagram of the process including automatic bone segmentation, kinematics quantification, and algorithm validation.

2.3.1 Initialization of Segmentation: Separation of Femur and Tibia

The quality of segmentation obtained is directly related to the quality of image registration. Thus to optimize the quality of image registration, the baseline and follow-up, the images must be separated according to each bone, and the unwanted regions such as air and soft tissue must be removed. These steps minimize the likelihood that the image registration algorithm mistakenly aligns tibia and femur to the incorrect bone or to surrounding soft tissue of similar

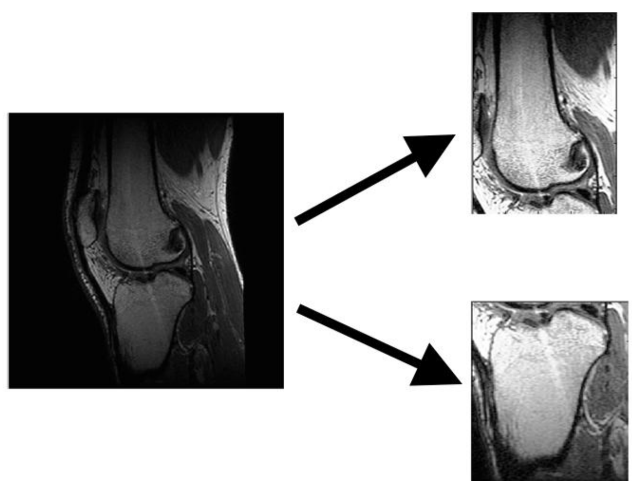

Figure 4: Example of MRI acquisition separated into femur and tibia, cropped, and normalized using histogram equalization

intensity. . In addition, once the cropped images are obtained, histogram equalization is applied to correct for potential regional intensity differences caused by coil sensitivity variation.

The key to separating the tibia and femur is finding the point along the superior-inferior axis that separates the two bones. In the T2-weighted fast spin echo images acquired, the bone marrow signal is bright while the joint space between the tibia and femur is dark. Taking the average intensity projection – the average voxel value along the sagittal plane Fig. 5b, reveals that there is a characteristic dark spot between the tibia and femur along the superior-inferior axis. The average-intensity projection can further be generalized into a one dimensional average intensity along the inferior-superior axis (Fig. 5a). The line plot demonstrates that there are two distinct peaks representing the thickest parts of the femur and tibia as well as a local minimum representing the joint space between them. Thus by identifying this characteristic local minimum, the approximate point of bone separation can be obtained. This approach was able to identify the joint space in over 99% of the cases tested, with the only exception being in images with acquisition error.

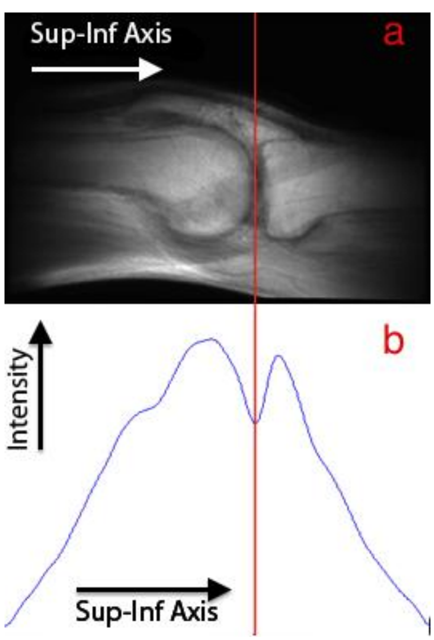

Figure 5:
(a) 2D Average Intensity Projection of 3D MRI Acquisition.
(b) Average Intensity of 2D projection along Superior-Inferior axis

Local minimum observed in the line plot reliably identifies the joint space between the tibia and the femur.

2.3.2 Image Registration

Once the baseline and followup images are partitioned into separate entities and the undesired portions of the images removed, the images are ready to be registered. The image registration operations were performed using software package *elastix* [6], an open-source tool that is applicable for many medical image registration problems. To effectively implement *elastix*, the user must specify a number of parameters for the image registration process. The most important parameters are the: cost function, transformation type, optimization scheme, sampling strategy, and interpolation type.

Cost Function

The cost function is the criteria for measuring similarity between the moving and fixed images to be registered. Simple criteria such as intensity and edge information can be used as well as more complicated criteria such as degree of bending or stretching. The cost function metric used for the application in this thesis was "Advanced Mattes Mutual Information", the default and recommended metric, which has been a popular choice in a number of medical imaging studies. [10-13].

Transformation

Next the transformation type must be determined. As previously mentioned, the two major categories are rigid and non-rigid transforms. *elastix* offers a variety of different transformation schemes, but the ones used in these methods are: 1) Euler transformation: a completely rigid transformation that only allows for translation and rotation, and 2) B-spline transform: a more complex non-rigid transform that allows for many local deformations.

Optimization:

To find the optimum registration, *elastix* offers a few different schemes. Adaptive Stochastic Gradient Descent, an extension of Robbins-Monro algorithm [14] was used in this segmentation method.

Sampling Strategies

When aligning a 3D image, it is useful to decrease the number of points sampled for computation time. Another useful feature implemented was limiting sampling points to a mask on the fixed image. This way the image registration will only optimize for the area of interest. The number of samples was set at 2048 per iteration. For the final registration, an approximate mask of the knee was used to exclude regions outside the area of interest.

Interpolation

Three-dimensional images will inherently have missing data in between slices. Therefore when registering, the non-voxel location intensity must be calculated using intensity interpolation. In this method, a 3^{rd} order B-spline intensity interpolation was used.

Hierarchical Strategies

An important feature used in this segmentation was hierarchical strategies, in which multiple iterations with increasingly complex parameters could be used to obtain the optimal transformation. In early iterations, low resolution, high filtering, and simple transforms (Euler) were used. In later iterations, high resolutions and a B-spline transformation model were used to obtain the final transformation. (Fig. 6).

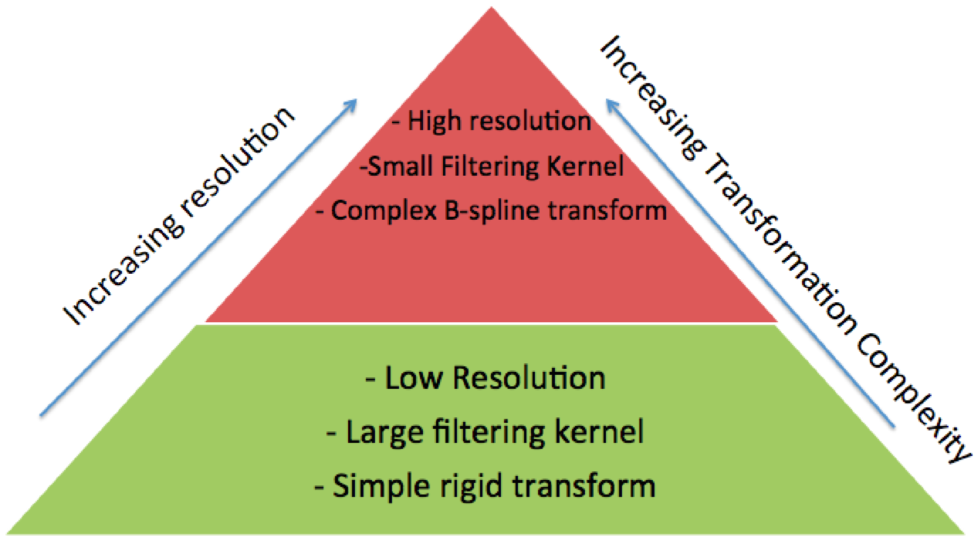

Figure 6. Hierarchical scheme for obtaining optimal registration

2.4 Quantification of Kinematics

Segmentations allow for the generation of 3D models to be used to quantify kinematics. Two key variables, Tibial Position (TP) and Internal Tibial Rotation (ITR) were obtained using in-house MatLab based software. This is the same process used in a previous study at UCSF [3].

Coordinate system for the bones was established using baseline contralateral knee (healthy). All follow-up knees were then registered to BL contralateral knee using iterative closest point method. Tibial Position (TP) was defined as the antero-posterior distance between the tibial and femoral origins established. Internal Tibial Rotation (ITR) was defined as the rotation of the tibia relative to the femur, with a more negative number indicating higher internal rotation.

2.5 Validation of Segmentation:

2.5.1 Visual Validation and Mathematical Similarity

Segmentation mask similarity using automatic and semi-automatic segmentation methods was obtained using the Jaccard index. The formal definition of the Jaccard index of two objects A and B is:

$$J(A,B) = \frac{A \cap B}{A \cup B} \tag{1}$$

where A and B are the automatic and semi-automatic masks, respectively. Two completely dissimilar images will have a Jaccard index of 0%, while two completely similar images will have a Jaccard index of 100% (Fig. 7). Segmentations that were found to have a low Jaccard index were visually inspected to validate the success or failure of the segmentation.

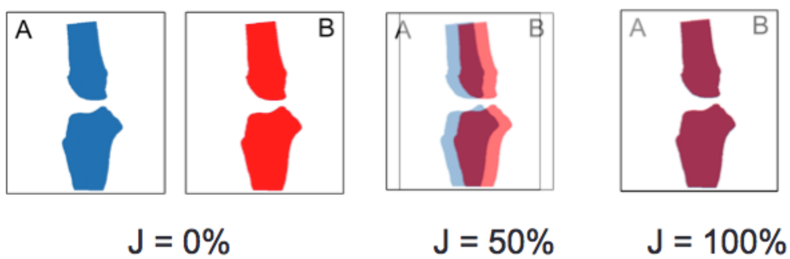

Figure 7. Example of Jaccard index values for different degrees of image similarity**.**

2.5.2 Kinematic Validation

In addition to validation at the mask level, the kinematic measures from the automatic segmentation were also validated. For reproducibility measurements, two types of comparisons were examined in the six healthy controls: differences between segmentations of two different acquisitions (scan/rescan), and differences between segmentations of the same image (process/re-processing). In both cases, the three groups of interest were: inter-operator differences, intra-operator differences, and automatic algorithm differences. Correlations and average absolute differences were observed for these comparisons.

For ACL-injured subjects, kinematic results from the automatic segmentation were compared to kinematic results from the semi-automatic segmentation. Average differences between the two groups and correlations were calculated. Paired t-test between the semi-automatic and automatic kinematics was performed to examine differences between two segmentation methods. Cross-sectional differences in TP and ITR between injured and the contralateral uninjured knees were compared at each time points using paired t-tests. Longitudinal differences in TP and ITR of injured knees and contralateral knees were also compared between follow up and baseline using paired t-tests. Significance was set at $P < 0.05$.

3. Results

3.1 Visual and Mathematical Validation

Bilateral segmentations of 30 subjects at 3 time points (6-month, 1-year and 2-year after ACL reconstruction) were obtained , a totaling 175 knees due to some missing follow-up points. Segmentation was successful in 173/175 (98.9%) of cases in ACL-reconstructed cohort. In general, segmentation of the central slices of images was well aligned with bone contours. In addition, segmentation proved to be successful for follow-up images that contained tunnel from ACL reconstruction. (Fig. 8).

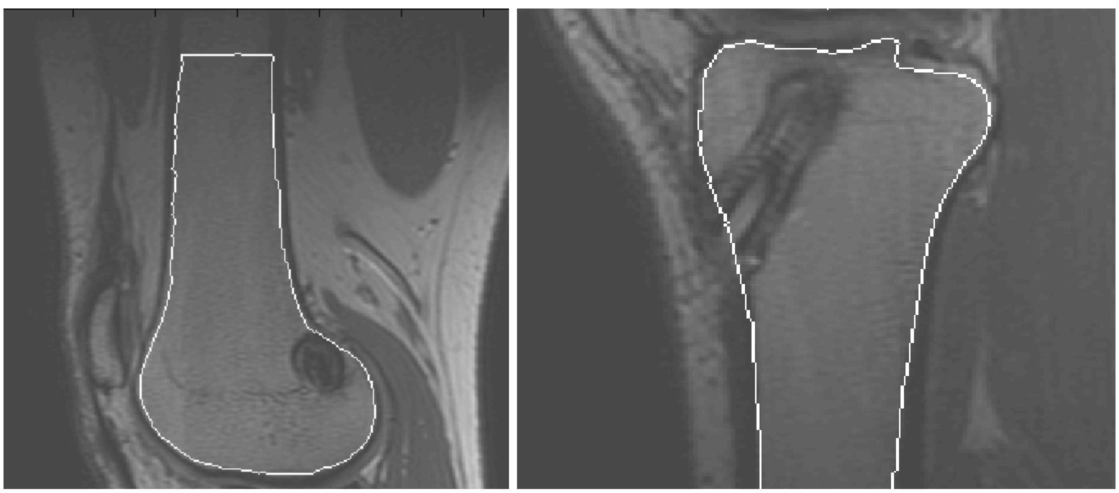

Figure 8. Automatic segmentation (outline marked in white) of ACL-reconstructed follow-up MRI

For 175 cases examined, including the failed segmentations, the average Jaccard index value was 85.1%. Values ranged from 71.3% (a failed case) to 91.5%. A histogram of the Jaccard indices is shown in Fig. 9. Comparisons between semi-automatic and automatic masks showed high alignment at the joint space, but different degrees of segmentation of the tibial and femoral shaft. (Fig.10).

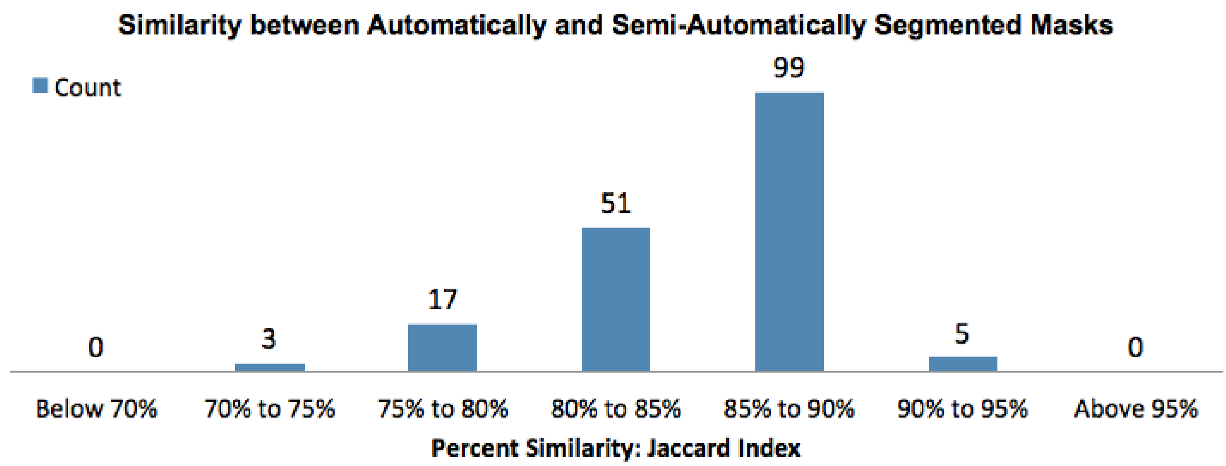

Figure 9. Similarity between Automatic and Semi-automatic masks using Jaccard index similarity metric. Total count was 175.

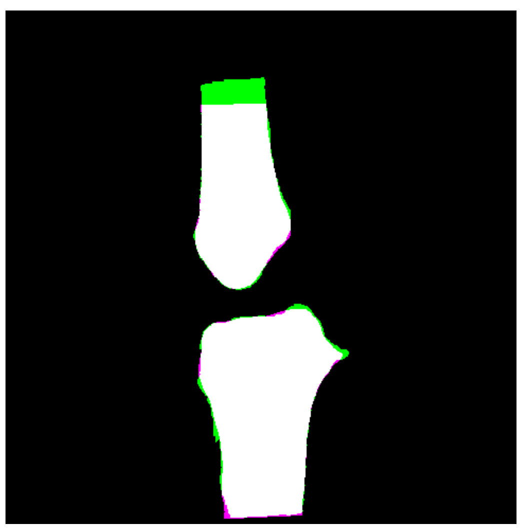

Figure 10. Overlay of automatic (green) and semi-automatic (magenta) masks. Aligned sections are shown in white

3.2 Reproducibility Kinematics

Scan/rescan Kinematic results

Automatic segmentation differences from scan/rescan kinematics were found to be lowest of the three groups, for both TP and ITR (Table 1). Intra-operator differences were found to be lower than inter-operator differences.

Table 1. Scan/rescan Comparisons for Tibial Position and Internal tibial rotation

Comparison Groups	Tibial Position Difference (mm)	ITR Difference (degrees)
Algorithm	0.46 +/- 0.41 mm	1.60 +/- 1.58 deg
Intra-operator	1.35 +/- 1.25 mm	1.70 +/- 1.45 deg
Inter-operator	1.47 +/- 1.23 mm	2.13 +/- 1.54 deg

Segment/Re-segment Results

Because the algorithm consistently produces the same result, the reprocessing difference in this approach is essentially 0. Intra-operator differences were found to be less than inter-operator differences for both TP and ITR (Table 2).

Table 2. Segment/Re-segment Comparisons for Tibial Position and Internal Tibial Rotation

Comparison Groups	TP: Average Absolute Difference (mm)	ITR: Average Absolute Difference (deg)
Algorithm	0	0
Intra-operator	0.37 +/- 0.48 mm	0.57 +/- 0.70 deg
Inter-operator	0.65 +/- 0.42 mm	1.37 +/- 0.99 deg

3.3 Automatic vs. Semi-Automatic Kinematics

Combining all time points and all knees, correlation between automatic and semi-automatic was above 0.9 for both TP and ITR (R = 0.935, and 0.900, respectively, Fig. 11, Table 3).

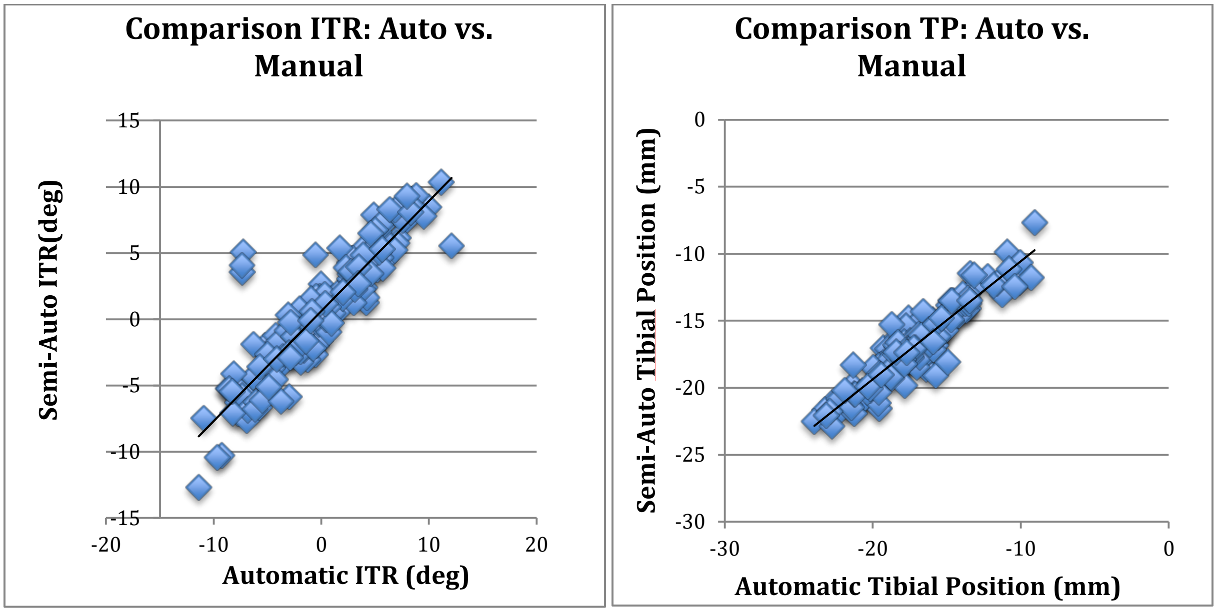

Figure 11. Comparisons between Automatic and Semi-Automatic Kinematics: Internal Tibial Rotation (left) and Tibial Position (right)

Table 3. Summary of Automatic vs. Semi-Automatic Results

	Correlation (R)	Average Difference
Tibial Position (TP)	0.935	0.83 +/- 0.72 mm
Internal Tibial Rotation (ITR)	0.900	1.45 +/- 1.74 deg

Longitudinal comparisons of injured vs. healthy knee (Fig. 12) TP is significantly more anterior in injured compared to healthy knee at baseline, 6-month, 1-year, and 2-year follow-up (p = 0.0011, p = 0.0036, p = 0.0055, p = 0.0002, respectively). Additionally, TP of healthy knee at 2-years is significantly more anterior than at baseline (p = 0.04). Injured knee was found to have significantly lower ITR at 2-years compared to at baseline (p = 0.02). Healthy knee was found to have significantly lower ITR in 6-months compared to baseline, 2-years compared to baseline, 2-years compared to 6-months, and 2-years compared to 1-year (p = 0.378, p = 0.0003, p = 0.0287, p = 0.0440, respectively).

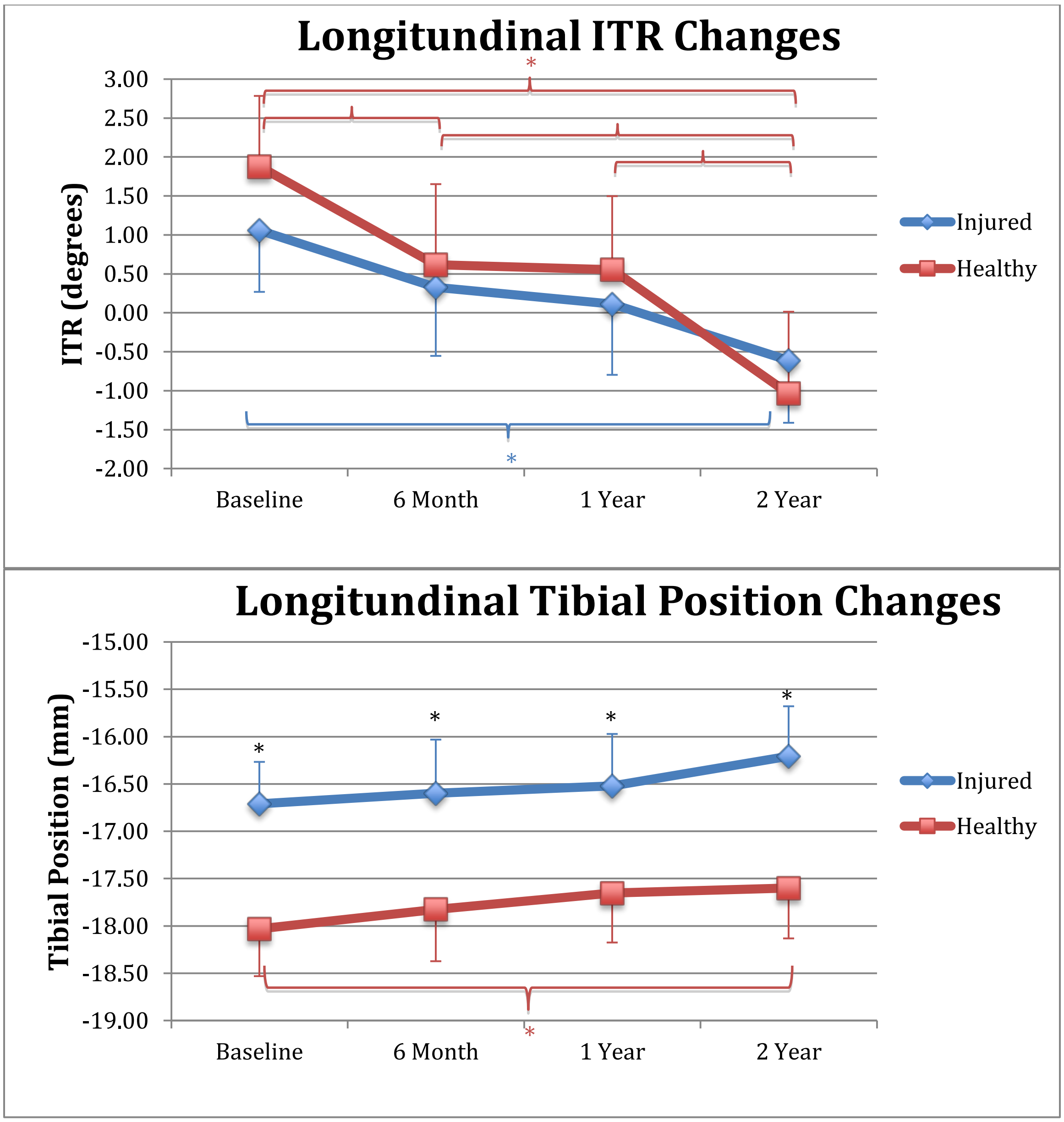

Figure 12. Longitudinal Changes in Kinematics over 2 years.
* Represents significant differences at given time points

4. Discussion

4.1 Visual Analysis

The success rate of segmentation (98.9% for 175 cases) demonstrates that the automatic segmentation technique is very robust. The registration approach was very beneficial because the assumption was that overall bone shape would not change dramatically over a one to two year period.

Initially the image registration step used whole images, including both tibia and femur, but this method was only successful in about 75% of the cases, produced overall lower quality segmentation, and had a longer runtime. By isolating the tibia and femur and removing parts of the image likely to cause errors in the registration process, the effect on segmentation quality was immediately apparent.

Another major contributing factor to image registration success was the normalization of bone length before registration. Even though baseline and follow-up acquisitions have the same field of view, they may not have the same center of image. In addition, differences in intensity throughout the image caused by coil placement may cause unequal distribution of intensity throughout the bones. This can cause significant problems in aligning two images. Normalizing the length of the bone and applying histogram correction drastically reduced the degree of misalignment after registration.

4.2 Challenges

Through visual inspection of masks, a few key challenges to the automatic segmentation algorithm were found. The 2 unsuccessful cases were recognized as failed segmentations upon examining the final masks obtained. For the two failed cases (Fig. 11), it is apparent that there is partial but incomplete alignment of the segmentation to the bone. The example in Fig. 11a shows that there is a darkened region at the tibia. This intensity bias was likely a contributing factor to failed registration. For future image acquisitions, it is suggested that MRI operators try to center the image as close to the baseline as possible. In addition, the receiving knee coil should be centered on the joint between the tibia and femur. One potential strategy to minimize intensity bias is through bias field correction MR techniques such as the widely used N3 Method [15]. This was not explored in the current study, but may prove to be very useful in future developments.

In both of these cases, there was partial but incomplete alignment of the segmentation to the bone (Fig. 11). In one case, shown in Fig. 11b, the femur was successfully segmented, but the tibia was unsuccessfully segmented. One potential reason is that the difference in intensity of tibia and femur between baseline and follow-up was too much to overcome. Additionally, because the images are registered using random sampling, there may have not been enough points sampled to obtain the optimal registration. Future implementations to approaches these tough cases are: use of bias-correction techniques as mentioned earlier, and increasing the number of sampled points.

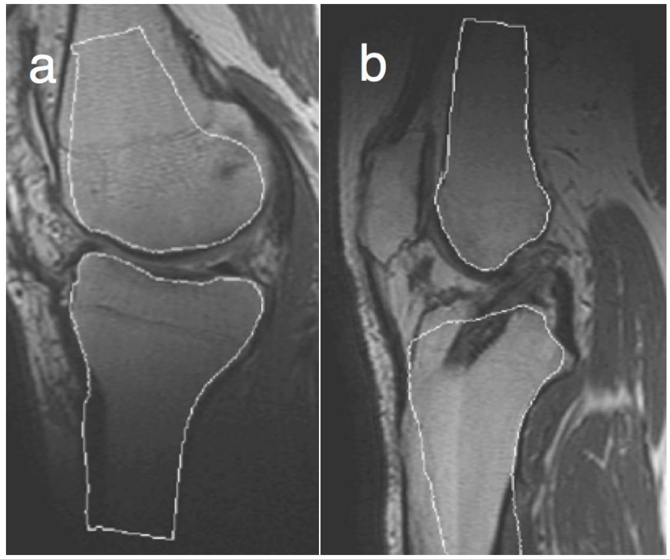

Figure 13. Single slice views of two failed segmentation cases

A few other notable challenges were inconsistent masks in edge slices, due to interpolation difficulties (Figs. 12a and 12b), problems in segmenting unclear boundaries (fig. 12c), and problems segmenting slices with partial volume artifacts (Fig. 12d).

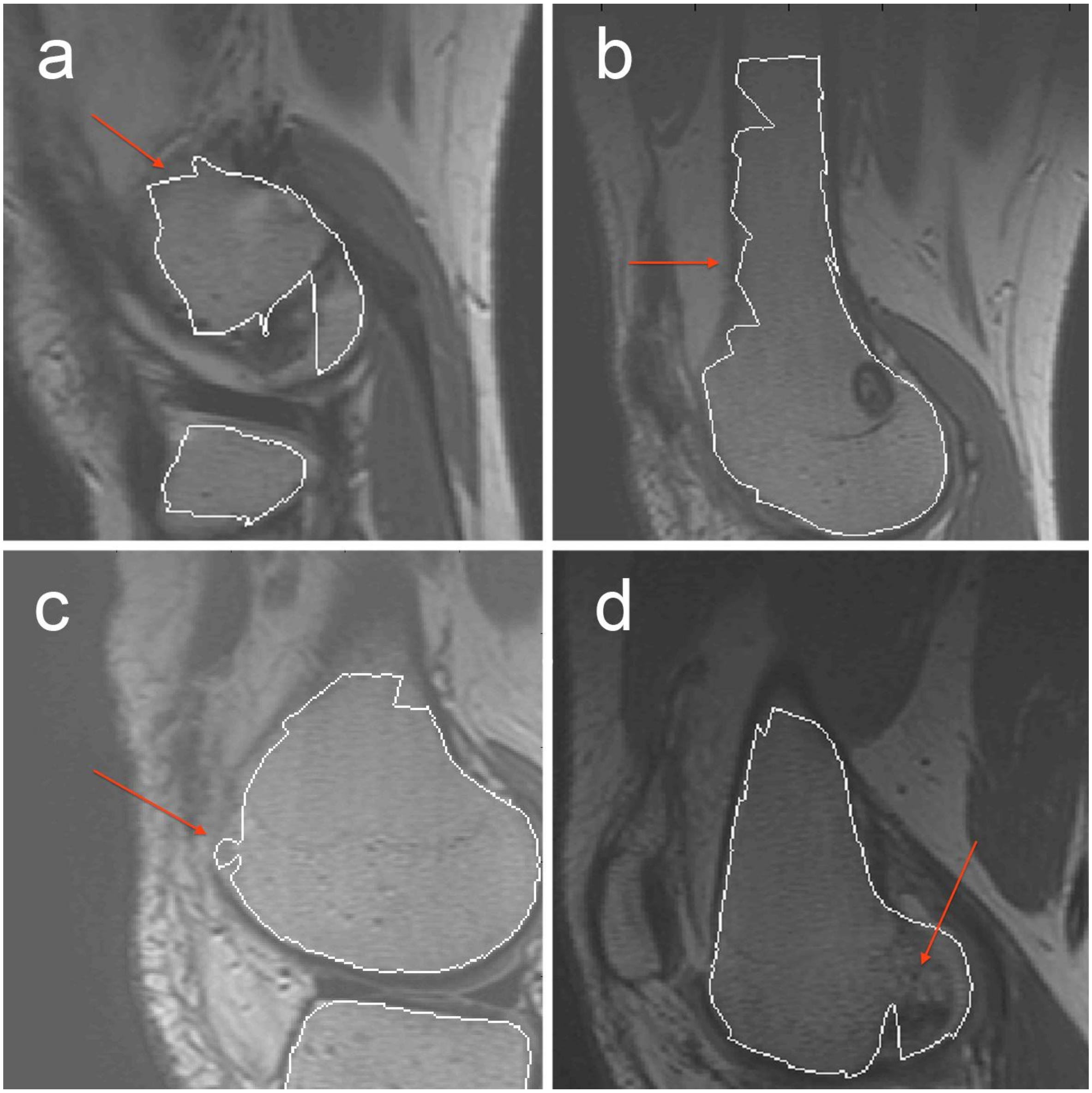

Figure 14. (a) Slice along the edge with edge interpolation difficulties. (b) A slice showing partial but incomplete segmentation due to interpolation (c) Local segmentation problems at an unclear boundary (d) Slice showing partial volume effect.

Missing image data between MRI slices is an inevitable problem when in-plane resolution (.39mm) is different than the slice thickness (1.5 mm). When transforming binary masks, this will produce “jagged edges” (Fig 12a and 12b) because the data in between is not accounted for. This phenomenon increases in slices farther from the center of the image.

Unclear boundaries of bone (Fig. 12c) were another challenge to the segmentation process. These boundaries are likely to cause confusion when images are registered, especially for the non-rigid transform. It is worth mentioning, however, that some boundaries are so ambiguous that non-automated approaches are also ineffective. Overall these ambiguous boundaries seemed to cause local deformations on certain slices but did not contribute to a dramatic change in overall shape of segmentation.

Lastly, segmentation of slices affected by partial volume effect proved difficult to segment. This phenomenon usually occurs when larger cross-section of bone is in an adjacent slice to a smaller bone cross-section. This often happens in the femur because of the gap in between the two condyles. For images used in this study, a slice with partial volume artifact will look like a blend between the larger and smaller bone cross-section (Fig. 12d). Generally, segmentation operators will either treat that slice as either one or the other, not a combination of both. The automatic segmentation technique has no way to resolve this situation, and produces segmentations that may not be ideal.

In future studies, to acquire MRI images with higher resolution, both in place and in slice direction will help to deal with challenges mentioned above and improve registration outcomes.

4.3 Mathematical Similarities between Automatic and Semi-Automatic Masks

In this study, a Jaccard index of above 80% was considered very good. However, the value of the Jaccard index can be potentially misleading. Because the length of the bone shafts in each image is not consistent, it may cause differences in Jaccard index when in fact the area of interest (at the joint) is actually very similar. However, the differences in bone shaft do not have a major impact on kinematic data, unlike the bone at the joint space. In some cases the Jaccard index was a low as 70% even though the overlap at the joint space was closely matching (Fig. 10). Histogram of similarity measurements (Fig. 9) shows that most segmentations fell within the 85 to 90% range. Given the discrepancy of the shaft in segmentations, this is a very promising result, indicating that automatic segmentations are consistently very similar to semi-automatic segmentations at the mask level.

4.4 Reproducibility of Kinematics

Automatic segmentation algorithm showed excellent reproducibility compared to that of the semi-automatic segmentations for scan/rescan. Average absolute difference between scan and rescan kinematics were found to be lowest in automatic segmentation for both Tibial Position and Internal Tibial Translation. This demonstrates that the algorithm is very consistent in the way that it segments follow up images. The strong similarity between the kinematics of the scan/rescan segmentations may be attributed to the 3D image registration framework. Because the input mask is transferred and transformed onto the follow up image, many of the spatial relationships between different slices are preserved. This does not hold true for current semi-automatic segmentations, in which every scan must be segmented slice by slice. Automatic segmentation could therefore be described as solving one three-dimensional problem, while semi-automatic and manual segmentations could be described as solving multiple two-dimensional problems.

4.5 Kinematic Automatic Vs. Semi-Automatic Differences

Comparisons between automatic and semi-automatic kinematics showed that there is a high degree of similarity between the two (Pearson's correlation coefficient: R = 0.935 for TP, R = 0.900 for ITR). This indicates that automatic methods are able to quantify kinematics in a similar fashion to the semi-automatic method, though not in the exact same way. Looking at the average absolute differences from Table 3 (TP: 0.83 +/- 0.72 mm, ITR: 1.45 +/- 1.74 deg), they are most similar to inter-operator differences for segment-resegment evaluation (TP: 0.65 +/- 0.42 mm, ITR: 1.37 +/- 0.99 deg). This suggests that the automatic segmentation algorithm behaves similarly to another operator.

Analysis of longitudinal data from automatic segmentations shows that there are changes in kinematics over two years. In both ITR and TP, there are significant changes that can be detected over two years. This is a promising result, and indicates that the automatic segmentation technique is consistent enough that significant differences can be detected. Though deeper clinical impact of these findings is not examined in this study, these preliminary findings show that the automatic segmentation method mentioned can be used as a means for observing clinically significant changes over time.

4.6 Future Directions

Given that there was considerable success in the quantification of kinematics using this segmentation method, it is worth attempting to apply the approach to generate data for other applications, such as analysis of bone shape. Previous studies have indicated bone shape as a variable of interest in premature osteoarthritic development [4]. However, bone shape analysis requires a higher degree of segmentation quality, which may not necessarily be attainable with the current setup.

Another potential segmentation approach that can stem from the current one is an inter-patient atlas-based registration [5] rather than the current intra-patient registration method. Using such a method will vastly expand the number of datasets that can be segmented. Segmentation quality would be expected to decrease, but this method could still prove to be very useful in future studies.

Lastly, the segmentation approach can potentially be used for other anatomy, such as cartilage. There is a great need for automated methods for many other medical applications. Atlas-based approaches may potentially be a solution to segmentation problems in these fields.

5. Conclusion:

The proposed automated segmentation algorithm provides a very time efficient method that can segment one knee in less than 5 minutes, as opposed to nearly 5 hours for current semi-automatic methods. The proposed method is also very consistent for reproducibility studies. Overall this method can be used as a reliable method for quantifying knee kinematics.

Bibliography

1. Lohmander, L. S., Englund, P. M., Dahl, L. L., & Roos, E. M. (2007). The long-term consequence of anterior cruciate ligament and meniscus injuries osteoarthritis. *The American journal of sports medicine*, *35*(10), 1756-1769.
2. Chaudhari, A. M., Briant, P. L., Bevill, S. L., Koo, S., & Andriacchi, T. P. (2008). Knee kinematics, cartilage morphology, and osteoarthritis after ACL injury.*Medicine and science in sports and exercise*, *40*(2), 215-222.
3. Lansdown, D. A., Zaid, M., Pedoia, V., Subburaj, K., Souza, R., Benjamin, C., & Li, X. (2014). Reproducibility measurements of three methods for calculating in vivo MR- based knee kinematics. *Journal of Magnetic Resonance Imaging*.
4. Pedoia, V., Lansdown, D. A., Zaid, M., McCulloch, C. E., Souza, R., Ma, C. B., & Li, X. (2015). Three-dimensional MRI-based statistical shape model and application to a cohort of knees with acute ACL injury. *Osteoarthritis and Cartilage*.
5. Kalinic, H. (2008). Atlas-based image segmentation: A Survey. *Department of Electronic Systems and Information Processing, Universiy of Zagreb*.
6. Klein, S., Staring, M., Murphy, K., Viergever, M., & Pluim, J. P. (2010). Elastix: a toolbox for intensity-based medical image registration. *Medical Imaging, IEEE Transactions on*, *29*(1), 196-205.
7. Georgoulis, A. D., Ristanis, S., Moraiti, C. O., Paschos, N., Zampeli, F., Xergia, S., ... & Mitsionis, G. (2010). ACL injury and reconstruction: Clinical related in vivo biomechanics. *Orthopaedics & Traumatology: Surgery & Research*, *96*(8), S119-S128.

8. Patel, V. V., Hall, K., Ries, M., Lotz, J., Ozhinsky, E., Lindsey, C., ... & Majumdar, S. (2004). A three dimensional MRI analysis of knee kinematics. *Journal of Orthopaedic Research*, *22*(2), 283-292.
9. Maes, F., Collignon, A., Vandermeulen, D., Marchal, G., & Suetens, P. (1997). Multimodality image registration by maximization of mutual information. *Medical Imaging, IEEE Transactions on*, *16*(2), 187-198.
10. Viola, P., & Wells III, W. M. (1997). Alignment by maximization of mutual information. *International journal of computer vision*, *24*(2), 137-154.
11. Mattes, D., Haynor, D. R., Vesselle, H., Lewellen, T. K., & Eubank, W. (2003). PET-CT image registration in the chest using free-form deformations. *Medical Imaging, IEEE Transactions on*, *22*(1), 120-128.
12. Thévenaz, P., & Unser, M. (2000). Optimization of mutual information for multiresolution image registration. *Image Processing, IEEE Transactions on*,*9*(12), 2083-2099.
13. Rueckert, D., Sonoda, L. I., Hayes, C., Hill, D. L., Leach, M. O., & Hawkes, D. J. (1999). Nonrigid registration using free-form deformations: application to breast MR images. *Medical Imaging, IEEE Transactions on*, *18*(8), 712-721.
14. Klein, S., Pluim, J. P., Staring, M., & Viergever, M. A. (2009). Adaptive stochastic gradient descent optimisation for image registration. *International journal of computer vision*, *81*(3), 227-239.
15. . Boyes, R. G., Gunter, J. L., Frost, C., Janke, A. L., Yeatman, T., Hill, D. L., ... & Fox, N. C. (2008). Intensity non-uniformity correction using N3 on 3-T

scanners with multichannel phased array coils. *Neuroimage*, *39*(4), 1752-1762.

Publishing Agreement

It is the policy of the University to encourage the distribution of all theses, dissertations, and manuscripts. Copies of all UCSF theses, dissertations, and manuscripts will be routed to the library via the Graduate Division. The library will make all theses, dissertations, and manuscripts accessible to the public and will preserve these to the best of their abilities, in perpetuity.

Please sign the following statement:

I hereby grant permission to the Graduate Division of the University of California, San Francisco to release copies of my thesis, dissertation, or manuscript to the Campus Library to provide access and preservation, in whole or in part, in perpetuity.

Samuel Huang

Author Signature

9/4/15

Date